Modification of Opal Photonic Crystals Using Al_2O_3 Atomic Layer Deposition

Z. A. Sechrist,[†] B. T. Schwartz,[‡] J. H. Lee,[‡] J. A. McCormick,[§] Rafael Piestun,[‡] W. Park,[‡] and S. M. George*[,§]

Department of Chemistry and Biochemistry, Department of Electrical Engineering, and Department of Chemical and Biological Engineering, University of Colorado at Boulder, Boulder, Colorado 80309

Received February 2, 2006. Revised Manuscript Received May 9, 2006

Aluminum oxide (Al_2O_3) atomic layer deposition (ALD) on synthetic opal was explored as a model system to understand the growth of ALD films on photonic crystals. Al_2O_3 ALD was used to coat the silica spheres in synthetic opal with conformal Al_2O_3 films. Using Al_2O_3 ALD to modify the interstices of the opal allowed for the tuning of the position and intensity of the Bragg reflection from the opal structure. Numerical transfer matrix method (TMM) simulations were used to predict the optical effects from the modified photonic crystal. The TMM simulations assumed an ideal face-centered cubic (fcc) crystal structure with conformal Al_2O_3 ALD on all surfaces. The experimental Bragg wavelengths from the Al_2O_3-coated photonic crystals were observed to shift to longer wavelength versus Al_2O_3 ALD thickness before asymptotically reaching a limiting wavelength. This red shift was attributed to the higher effective refractive index produced when Al_2O_3 ALD coats the SiO_2 spheres in the opal structure. The experimental and predicted Bragg wavelengths showed excellent agreement for thin Al_2O_3 ALD films. This agreement indicated that the Al_2O_3 ALD inside of the opal structure occurs conformally as assumed by the model. Differences between experiment and simulation were observed for high filling fractions of the opal structure. These discrepancies were attributed to a higher free volume in the opal structure than the free volume predicted by the fcc geometry. The reflectance of the Bragg peak also decreased versus Al_2O_3 ALD thickness. This reduction in intensity was attributed to the decrease in the refractive index difference between the SiO_2 spheres and their surroundings.

I. Introduction

Photonic crystals are periodic structures that can be tailored to alter the reflection, absorption, emission, and transmission of electromagnetic radiation. Photonic crystals at optical frequencies have generated wide interest for their applications in optoelectronics,[1] sensing,[2] and energy conversion.[3] These periodic structures can lead to strong inhibition of light propagation at certain wavelengths. The range of forbidden propagating wavelengths within the crystal is known as a photonic band gap. A complete band gap prevents light propagation in all directions and may be possible if there is sufficient contrast between the high and the low refractive index regions of the photonic crystal.[4,5]

Photonic band engineering has recently become a high priority because of its potential use in slowing down the group velocity of light,[6] focusing,[7] guiding,[8] and storing light.[9] However, fabrication of three-dimensional photonic crystals has lagged behind theoretical developments and two-dimensional demonstrations. The demonstration of photonic crystals in the visible has proved challenging, and the fine-tuning of the band structure requires innovative approaches. In this paper, we address this problem by modifying a photonic crystal matrix using Al_2O_3 atomic layer deposition (ALD).

Synthetic opals have been produced with high degrees of regularity and dimensional control.[10,11] In these synthetic opals, silica spheres are self-assembled into a close-packed colloidal crystal. The geometry of the system allows the structure to act as a photonic crystal.[12] However, large refractive index differences between the high and the low index materials in the system must be achieved to produce a complete three-dimensional photonic band gap. For example, the refractive index of the dielectric must be $n > 2.8$ for a face-centered cubic (fcc) lattice of air spheres in a

[†] Department of Chemistry and Biochemistry.
[‡] Department of Electrical Engineering.
[§] Department of Chemical and Biological Engineering.

(1) Arsenault, A.; Fournier-Bidoz, S. B.; Hatton, B.; Miguez, H.; Tetrault, N.; Vekris, E.; Wong, S.; Yang, S. M.; Kitaev, V.; Ozin, G. A. *J. Mater. Chem.* **2004**, *14*, 781.
(2) Chow, E.; Grot, A.; Mirkarimi, L. W.; Sigalas, M.; Girolami, G. *Opt. Lett.* **2004**, *29*, 1093.
(3) Sai, H.; Yugami, H. *Appl. Phys. Lett.* **2004**, *85*, 3399.
(4) John, S. *Phys. Rev. Lett.* **1987**, *58*, 2486.
(5) Yablonovitch, E. *Phys. Rev. Lett.* **1987**, *58*, 2059.
(6) Soljacic, M.; Johnson, S. G.; Fan, S. H.; Ibanescu, M.; Ippen, E.; Joannopoulos, J. D. *J. Opt. Soc. Am. B* **2002**, *19*, 2052.
(7) Pendry, J. B. Intense Focusing of Light Using Metals. In *Photonic Crystals and Light Localization in the 21st Century*; Soukoulis, C. M., Ed.; Kluwer Academic Publishers: Dordrecht, The Netherlands, 2000; p 329.
(8) Mekis, A.; Chen, J. C.; Kurland, I.; Fan, S. H.; Villeneuve, P. R.; Joannopoulos, J. D. *Phys. Rev. Lett.* **1996**, *77*, 3787.
(9) Yanik, M. F.; Suh, W.; Wang, Z.; Fan, S. *Phys. Rev. Lett.* **2004**, *93*, 233903.
(10) Comoretto, D.; Grassi, R.; Marabelli, F.; Andreani, L. C. *Mater. Sci. Eng. C* **2003**, *23*, 61.
(11) Lopez, C.; Vazquez, L.; Meseguer, F.; Mayoral, R.; Ocana, M.; Miguez, H. *Superlattices Microstruct.* **1997**, *22*, 399.
(12) Krauss, T. F.; De la Rue, R. M. *Prog. Quantum Electron.* **1999**, *23*, 51.

10.1021/cm060263d CCC: $33.50
Published on Web 06/29/2006

dielectric matrix.[13,14] The refractive index of silica is not large enough to create a photonic band gap because $n_{SiO_2} = 1.43$.

To increase the refractive index difference, the voids between the silica spheres in the opal structure can be filled with a high-index material. A large number of infiltration techniques have been investigated previously, such as thermal decomposition,[15] spray pyrolysis,[16] chemical vapor deposition (CVD),[17] electroless plating,[18] and ceramic fabrication techniques.[19] ALD has also recently been introduced as a technique for conformal deposition on the colloidal crystals.[20−24]

The ability to control thickness and conformality of the coatings deposited inside of the opal structure strongly affects the optical properties of the photonic crystal. Theoretical work has suggested that less than complete filling of the free volume in the opal leads to gap size enhancement.[14] Conformal deposition on the silica spheres would produce a highly regular lattice of small air voids between the coated spheres. This type of growth is expected for ALD inside of a packed bed of spheres.[25] Low index of refraction bridges between the spheres may also improve gap size enhancement.[14] These low index of refraction materials may also be deposited via ALD techniques.

ALD can grow conformal films of a wide variety of materials.[26] ALD is a subset of CVD and is based on sequential, self-limiting surface reactions.[27] The substrate is only exposed to one reactant at a time. This temporal separation eliminates gas-phase reactions and allows every available surface site to react with sufficient exposures.[27] After every available site has reacted with the first precursor, the reaction stops in a self-limiting fashion. The precursor can then be purged from the reactor, and the next precursor can be exposed to the new surface sites on the substrate. ALD has shown conformal coverage on substrates that have high aspect ratios[28] and tortuous precursor delivery paths.[29]

Al_2O_3 ALD is an ideal system that has been studied more extensively than any other ALD system.[27,30,31] Al_2O_3 ALD exhibits extremely continuous, conformal, and pinhole-free film growth.[32,33] In addition, there is rapid nucleation and very predicable growth rates for Al_2O_3 ALD. Unfortunately, Al_2O_3 ALD has a relatively low refractive index of $n_{Al_2O_3} = 1.65$.[31] This low refractive index will not produce a band gap after filling the free volume in the opal structure. However, Al_2O_3 ALD on opal can be studied as a model system to understand the effect of ALD on opal.

In this paper, Al_2O_3 ALD on opal was optically monitored as the fill fraction of Al_2O_3 ALD in the opal voids changed from 0 to near 100%. The Bragg reflection position was compared with numerical predictions from the transfer matrix method (TMM)[34,35] and the more simplified predictions from the Bragg−Snell relation.[11,36,37] The growth patterns of the Al_2O_3 ALD film inside of the synthetic opal structure were also monitored using scanning electron microscopy (SEM). The understanding of ALD inside of opal templates was tested by comparing the experimental Bragg wavelengths with the Bragg wavelengths predicted by the TMM simulations. The discrepancies between the measured and predicted Bragg wavelengths helped characterize the deviations of the synthetic opals from the ideal fcc structure.

II. Experimental Section

A. Al_2O_3 ALD on Opal. Al_2O_3 ALD thin films were deposited on opal in a hot wall viscous flow reactor. The reactor has been described in detail previously.[38] Nitrogen (99.999% pure; Air Gas, Inc., ultrahigh purity (UHP)) was used as the carrier and purge gas. The total pressure in the growth region was ~1 Torr with a flow velocity of ~1 m/s. The reactant gases were pulsed into the nitrogen flow with computer controlled pneumatic valves (Swagelok). The reactant gas was entrained in the nitrogen flow and transported through the reactor. After the gas reacted to completion with the available surface sites, the nitrogen entrained the excess reactant and products. A purge time after each reactant exposure allowed for the nitrogen to sweep the reactor clean of reactive gases.

The ALD reactor was heated to 125 °C using a ceramic Watlow heating system. The trimethylaluminum (TMA) and H_2O reactants for Al_2O_3 ALD were all kept at room temperature. The pressures of TMA and H_2O at room temperature are 9 Torr[39] and 18 Torr,[40]

(13) Sozuer, H. S.; Haus, J. W.; Inguva, R. *Phys. Rev. B* **1992**, 45, 13962.
(14) Busch, K.; John, S. *Phys. Rev. E* **1998**, *58*, 3896.
(15) Golubev, V. G.; Kosobukin, V. A.; Kurdyukov, D. A.; Medvedev, A. V.; Pevtsov, A. B. *Semiconductors* **2001**, *35*, 680.
(16) Abrarov, S. M.; Yuldashev, S. U.; Lee, S. B.; Kang, T. W. *J. Lumin.* **2004**, *109*, 25.
(17) Miguez, H.; Chomski, E.; Garcia-Santamaria, F.; Ibisate, M.; John, S.; Lopez, C.; Meseguer, F.; Mondia, J. P.; Ozin, G. A.; Toader, O.; van Driel, H. M. *Adv. Mater.* **2001**, *13*, 1634.
(18) Wen, W. J.; Wang, N.; Zheng, D. W.; Chen, C.; Tu, K. N. *J. Mater. Res.* **1999**, *14*, 1186.
(19) Subramania, G.; Constant, K.; Biswas, R.; Sigalas, M. M.; Ho, K. M. *Appl. Phys. Lett.* **1999**, *74*, 3933.
(20) King, J. S.; Graugnard, E.; Summers, C. J. *Adv. Mater.* **2005**, *17*, 1010.
(21) King, J. S.; Neff, C. W.; Summers, C. J.; Park, W.; Blomquist, S.; Forsythe, E.; Morton, D. *Appl. Phys. Lett.* **2003**, *83*, 2566.
(22) Scharrer, M.; Wu, X.; Yamilov, A.; Cao, H.: Chang, R. P. H. *Appl. Phys. Lett.* **2005**, *86*, 151113.
(23) Rugge, A.; Becker, J. S.; Gordon, R. G.; Tolbert, S. H. *Nano Lett.* **2003**, *3*, 1293.
(24) Rugge, A.; Park, J. S.; Gordon, R. G.; Tolbert, S. H. *J. Phys. Chem. B* **2005**, *109*, 3764.
(25) Ferguson, J. D.; Weimer, A. W.; George, S. M. *Appl. Surf. Sci.* **2000**, *162*, 280.
(26) Ritala, M.; Leskela, M. Atomic Layer Deposition. In *Handbook of Thin Film Materials*; Nalwa, H. S., Ed.; Academic Press: San Diego, 2001; Vol. 1, Chapter 2.
(27) George, S. M.; Ott, A. W.; Klaus, J. W.; *J. Phys. Chem.* **1996**, *100*, 13121.
(28) Elam, J. W.; Routkevitch, D.; Mardilovich, P. P.; George, S. M. *Chem. Mater.* **2003**, *15*, 3507.
(29) Mayer, T. M.; Elam, J. W.; George, S. M.; Kotula, P. G.; Goeke, R. S. *Appl. Phys. Lett.* **2003**, *82*, 2883.
(30) Dillon, A. C.; Ott, A. W.; Way, J. D.; George, S. M. *Surf. Sci.* **1995**, *322*, 230.
(31) Ott, A. W.; Klaus, J. W.; Johnson, J. M.; George, S. M. *Thin Solid Films* **1997**, *292*, 135.
(32) Groner, M. D.; Elam, J. W.; Fabreguette, F. H.; George, S. M. *Thin Solid Films* **2002**, *413*, 186.
(33) Ritala, M.; Leskela, M.; Dekker: J. P.; Mutsaers, C.; Soininen, P. J.; Skarp, J. *Chem. Vap. Deposition* **1999**, *5*, 7.
(34) Reynolds, A. L. *Translight Software*; University of Glasgow: Glasgow, U.K., 2000.
(35) Bell, P. M.; Pendry, J. B.; Moreno, L. M.; Ward, A. J. *Comput. Phys. Commun.* **1995**, *85*, 306.
(36) Compton, A. H. *X-rays in theory and experiment*; D. Van Nostrand Co., Inc.: New York, 1935.
(37) Ritchmyer, F. K.; Kennard, E. H. *Introduction to modern physics*, 3rd ed.; McGraw-Hill: New York, 1942.
(38) Elam, J. W.; Groner, M. D.; George, S. M. *Rev. Sci. Instrum.* **2002**, *73*, 2981.
(39) Bridgeman, O. C.; Aldrich, E. W. *J. Heat Transfer* **1964**, *86*, 279.

respectively. The reactants had a higher vapor pressure than the 1 Torr pressure in the reactor and could easily be dosed using pressure gradients. The ALD Al_2O_3 chemistry has been studied extensively and is as follows:[27,30,31]

$$\text{(A)}\quad \text{AlOH*} + \text{Al(CH}_3\text{)}_3 \rightarrow \text{AlOAl(CH}_3\text{)}_2\text{*} + \text{CH}_4 \qquad (1)$$

$$\text{(B)}\quad \text{Al(CH}_3\text{)*} + \text{H}_2\text{O} \rightarrow \text{AlOH*} + \text{CH}_4 \qquad (2)$$

where the asterisks indicate the surface species. Each AB cycle deposits 1.1−1.2 Å of Al_2O_3 per AB cycle at 177 °C.[31,32] The total film thickness is controlled by the number of AB cycles.

Synthetic opal is a highly ordered template. Like its natural counterpart, synthetic opal is composed of silica spheres assembled in close-packed fashion. Without any modification, both synthetic and natural opals create brilliant reflections that can vary in color at different angles of view. This property is known as opalescence. The silica spheres can be produced using the Stöber method.[41] This technique produces high yields of monodisperse silica spheres with a narrow diameter distribution of ±5%.

The spheres can then be allowed to self-assemble via the convective self-assembly technique.[42] This procedure allows the spheres to self-assemble into the close-packed opal structure that may be used as a periodic template for photonic crystals. The spheres organize on a glass substrate as they precipitate out of an ethanol solution that is 1 wt % of the silica spheres. The glass substrates were hung vertically in a beaker of ethanol solution. The beaker was exposed to ambient conditions, and the spheres were deposited during solvent evaporation. The solution was allowed to evaporate for 48 h. This evaporation time left ~1 cm of vertical deposition that was ~2.5 μm thick. After the samples had been deposited, they were sintered at 600 °C for 6 h to strengthen the structure.

The first attempt at Al_2O_3 ALD displayed very long nucleation periods that was atypical for Al_2O_3 ALD.[32] This long nucleation was attributed to outgassing from the opal samples. To avoid outgassing, a chemical cleaning procedure was adopted for the opal samples.[43] The samples were suspended in a 50/50 methanol (HPLC Burdick & Jackson)/hydrochloric acid (37% Mallinckrodt) mixture for 30 min. The samples were then rinsed with deionized water and subsequently suspended in sulfuric acid (51% Mallinckrodt) for 30 min. The samples were then rinsed with deionized water and dried with 99.9% nitrogen (USP grade, Air Gas).

B. Measurement of Al_2O_3 ALD on Opal and Reference Substrates. The mass changes during Al_2O_3 ALD were monitored using a quartz crystal microbalance (QCM). These QCM experiments were performed using a Maxtek TM 400 thickness monitor. The small changes in the oscillatory period were converted into mass per area using the Sauerbrey equation.[44] The mass per area and density yields the film thickness. UHP nitrogen was flown into the backside of the crystal housing to prevent backside deposition on the quartz sensor. These modifications have been discussed previously in detail.[45]

X-ray reflectivity (XRR) was used to measure Al_2O_3 ALD film thicknesses on reference substrates. XRR data was collected on a Bede Scientific D1 instrument. The filament current was 30 mA, and the accelerating voltage was 35 kV. The Al_2O_3 ALD thicknesses were determined through data fitting by the REFS genetic algorithm program (Bede Scientific). The films were grown on the substrates that were used as substrates for the opal. The substrates were Premium microscope slides (Fisher Scientific). Prior to growth, the glass slides were cleaned using an identical procedure as the procedure used to clean the opal.

SEM was used to image the uncoated and Al_2O_3 ALD-coated opals. The SEM instrument was a JEOL JSM-6400 microscope. The instrument was equipped with digital image processing and could resolve spatial features as small as 34 Å. The objective aperture used was 50 μm. Each sample was sputter-coated with ~50 Å of platinum prior to measurement to avoid sample charging. The operating voltage was 40 keV.

Atomic force microscope (AFM) measurements were performed using an Autoprobe CP instrument from Thermomicroscopes atop an air table (Integrated Dynamics Engineering). AFM images were acquired in noncontact mode. The tips were "B tips" on noncontact ultralevers (Thermomicroscopes, Inc.). All scans were 2×2 μm^2 and were performed at a scan rate of 0.1 Hz. Flattening with a second-order fitting for the fast scan direction and a first-order fitting for the slow scan direction was used to compensate for the distortion of the piezoelectric scanners.

All reflectance measurements were performed on a Cary 2400 ultraviolet−visible−near-infrared spectrometer (Varian, Inc.). The absolute specular reflectance accessory was used in the "VW" configuration. There was a single bounce reflection off of the sample at a near normal incidence. The reflectance measurements were performed through the backside of the glass slide. Performing the measurements through the backside of the sample avoided scattering from the opal surface roughness on the front side of the sample.

C. Numerical Simulations and Bragg−Snell Predictions. The TMM was used to predict the Bragg peak locations. The Translight program[34,35] was utilized to run TMM calculations to determine the predicted optical properties of the modified photonic crystals. The calculations assumed that the SiO_2 spheres were packed in a fcc lattice. In addition, the Al_2O_3 ALD was assumed to grow conformally on each sphere. The Al_2O_3 ALD coatings had a refractive index of 1.65.[31] A matrix of possible silica refractive indices and sphere sizes showed that the uncoated opal was best described by a silica refractive index of $n_{SiO_2} = 1.43$ and a silica sphere diameter of $d = 265$ nm.

The Bragg wavelength and wavelength shift with Al_2O_3 ALD coating can also be estimated within certain approximations via the Bragg−Snell equation:[11,36,37]

$$\lambda = (2a/m)(\mu^2 - \sin^2 \Theta)^{1/2} \qquad (3)$$

where λ is the wavelength of the maximum intensity of the Bragg peak. In this equation, the spacing between the (111) planes in the fcc crystal is a, where $a = (2/3)^{1/2}d$. The diameter of the silica spheres is d. The reflection order is $m = 1$, and the refractive index contrast between the effective refractive index of the opal structure and air is $\mu = n_{eff}/n_{air}$. The incident angle as measured from the normal is very close to $\Theta = 0$. Because $\sin^2 \Theta \sim 0$ and $n_{air} \sim 1.0$, eq 3 can be simplified to

$$\lambda = 2an_{eff} \qquad (4)$$

The wavelength of light is larger than the local spatial variations of the index of refraction. The effective index of refraction, n_{eff}, can be estimated as the average index of refraction:

$$n_{eff} = n_{SiO_2}F_{SiO_2} + n_{Al_2O_3}F_{Al_2O_3} + n_{air}F_{air} \qquad (5)$$

The refractive index of SiO_2 is n_{SiO_2}. The refractive index of Al_2O_3 is $n_{Al_2O_3}$. In addition, the fraction of SiO_2 is F_{SiO_2}, the fraction of

(40) McCullough, J. P.; Messerly, J. F.; Moore, R. T.; Todd, S. S. *J. Phys. Chem.* **1963**, *67*, 677.
(41) Stober, W.; Fink, A.; Bohn, E. *J. Colloid Interface Sci.* **1968**, *26*, 62.
(42) Jiang, P.; Bertone, J. F.; Hwang, K. S.; Colvin, V. L. *Chem. Mater.* **1999**, *11*, 2132.
(43) Cras, J. J.; Rowe-Taitt, C. A.; Nivens, D. A.; Ligler, F. S. *Biosens. Bioelectron.* **1999**, *14*, 683.
(44) Sauerbrey, G. Z. *Z. Phys.* **1959**, *155*, 206.
(45) Rocklein, M. N.; George, S. M. *Anal. Chem.* **2003**, *75*, 4975.

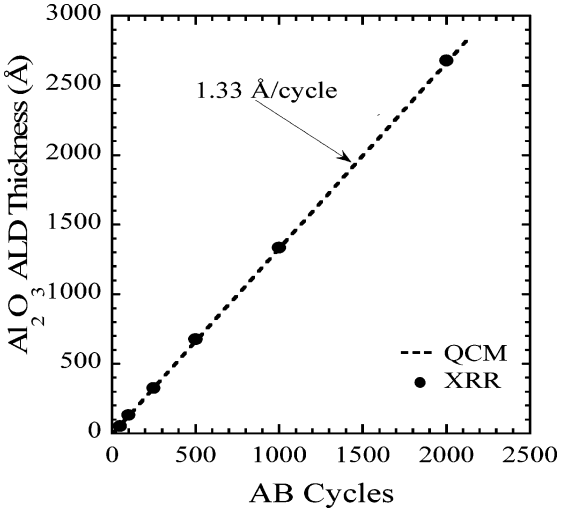

Figure 1. Al_2O_3 ALD film thickness on the microscope slide versus number of AB cycles measured using the QCM and XRR measurements.

Al_2O_3 is $F_{Al_2O_3}$, and the fraction of air is F_{air}. All of the space available in the opal consists of SiO_2, Al_2O_3, and/or air. All of the fractions must sum to unity, that is, $1 = F_{SiO_2} + F_{Al_2O_3} + F_{air}$. Consequently, the fraction of the volume of the structure occupied by Al_2O_3 ALD can be determined from the measured n_{eff} assuming that $F_{Al_2O_3} = 0$ prior to any Al_2O_3 ALD and $F_{air} = 0$ at the highest Al_2O_3 volume fraction.

A Monte Carlo simulation was used to predict the volume fraction in the opal structure that was filled by the Al_2O_3 ALD coating or the original silica spheres. Fourteen points were generated in a fcc arrangement (eight on the corners, six centered on the faces of the cube). Defining a radius centered on each lattice point simulates conformal Al_2O_3 ALD growth on the initial opal matrix. Sample points were randomly generated throughout the cube and rejected if they existed outside any sphere centered on the fcc lattice points. The Monte Carlo rejection fraction approaches the free volume fraction of the lattice after thousands of trials. As expected, the free volume fraction of the original fcc lattice was determined to be 0.26.

III. Results

Figure 1 shows XRR data for the ALD Al_2O_3 thicknesses versus the number of AB cycles. The Al_2O_3 ALD produces linear growth on flat substrates. The measured XRR thicknesses correlate well with the thickness measured with the QCM using a density of $\rho = 3.0$ g/cm^3. The thicknesses determined by the QCM measurements are shown in Figure 1 by the dotted line. The measured Al_2O_3 ALD growth rate is 1.33 Å per cycle. This rate is in reasonable agreement with previous literature for ALD Al_2O_3 ALD growth at 125 °C.[46] The *y* intercept is very close to 0, which indicates that Al_2O_3 ALD has no nucleation difficulties.

A SEM image of uncoated opals is shown in Figure 2. The SiO_2 spheres are observed as distinct individual spheres stacked, within domains, in a fcc structure. The silica sphere diameter is 255 ±13 nm. The sample cleaved unevenly and led to spheres in multiple planes being observed in the image. A SEM image of the opal after 1000 AB cycles of Al_2O_3 ALD is shown in Figure 3. The 1000 AB cycles are equivalent to an Al_2O_3 ALD film thickness of 1330 Å. Figure 3 shows no air voids between the spheres.

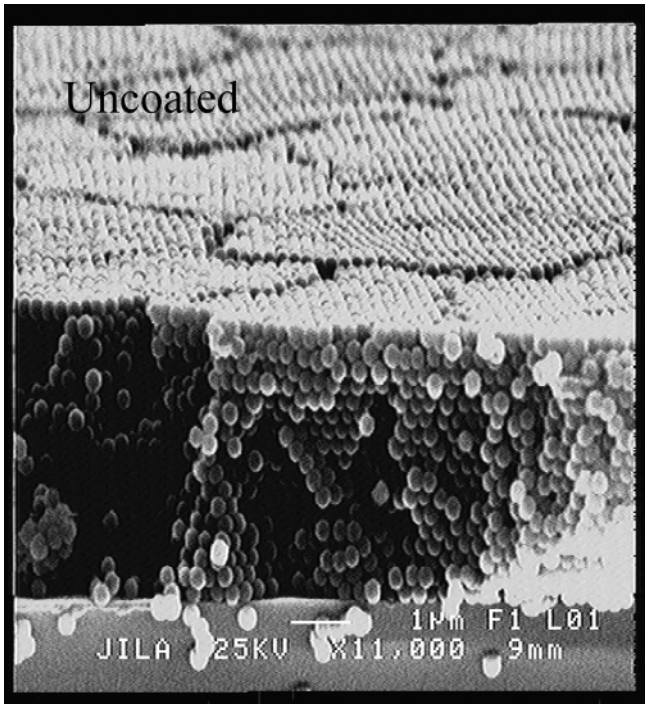

Figure 2. Scanning electron microscope image of an uncoated opal film on the microscope slide. Individual SiO_2 spheres with diameters of $d = 255 \pm 13$ nm are observed in a close-packed arrangement.

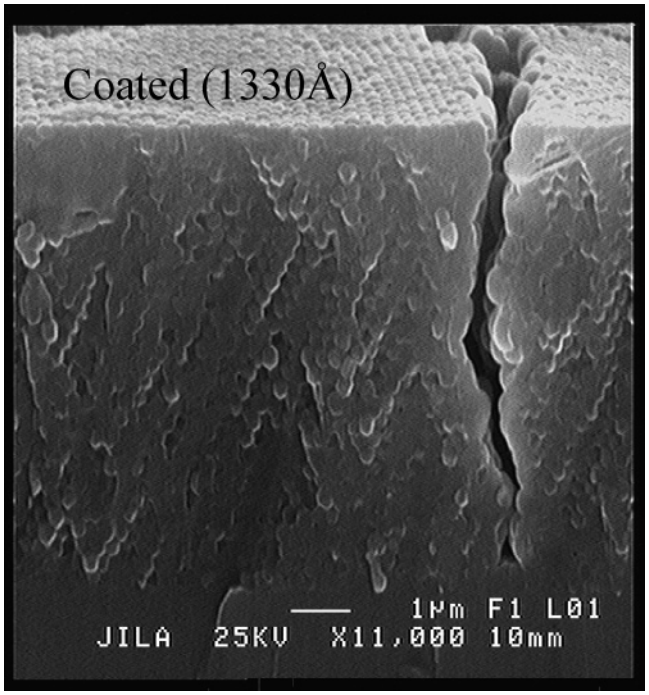

Figure 3. Scanning electron microscope image of an opal film coated with Al_2O_3 ALD after 1000 AB cycles. These 1000 AB cycles will produce an Al_2O_3 ALD film with a thickness of 1330 Å on a flat reference substrate.

Fissures are present in both SEM images. Fissures are created by thermal stress generated during the sintering process and have been previously discussed.[47,48] The SEM image in Figure 3 was not able to differentiate between the

(46) Groner, M. D.; Fabreguette, F. H.; Elam, J. W.; George, S. M. *Chem. Mater.* **2004**, *16*, 639.
(47) Comoretto, D.; Cavallo, D.; Dellepiane, G.; Grassi, R.; Marabelli, F.; Andreani, L. C.; Brabec, C. J.; Andreev, A.; Zakhidov, A. A. *Mater. Res. Soc. Symp. Proc.* **2002**, *708*, 317.

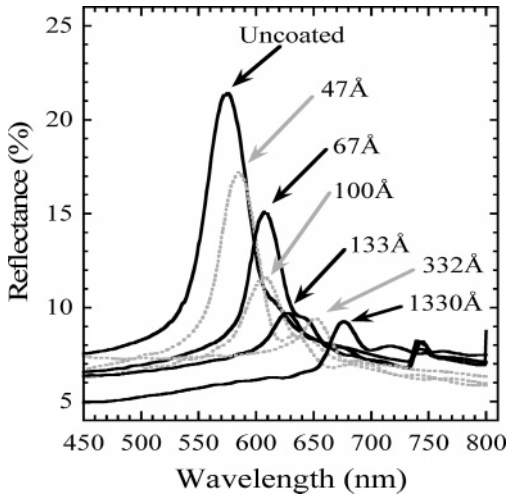

Figure 4. Reflectance from the opal structures versus wavelength. The Bragg peaks progressively shift to longer wavelength and decrease in intensity versus Al_2O_3 ALD thickness.

Al_2O_3 ALD coating and the SiO_2 spheres. The Al_2O_3 ALD conformally coats the SiO_2 spheres and allows the underlying surface corrugation to be observed on the top surface of the coated opal. The Al_2O_3 ALD coating does not have a gradient between the top and bottom of the opal structure. This uniformity indicates that the Al_2O_3 ALD coating is uniform throughout the opal structure.

Reflectance measurements were performed to observe the effect of Al_2O_3 ALD on the optical properties of the opal structure. Figure 4 displays the average reflectance spectra for opals coated with varying amounts of Al_2O_3 ALD. Each spectrum is an average of at least two spectra taken on different samples grown under identical conditions. The Bragg peak was produced by constructive reflections from various layers in the infiltrated opal structure. The original Bragg peak for the uncoated opal structure was at $\lambda = 576$ nm. The peaks shifted to longer wavelengths with the addition of the higher refractive index Al_2O_3 ALD. The progressive red shift in wavelength with Al_2O_3 ALD thickness is predicted by eq 4.[11]

Figure 5 compares the observed Bragg wavelength shifts with the wavelength shifts predicted by the TMM simulations. The experimental measurements and TMM simulations are very close for small Al_2O_3 ALD thicknesses. The TMM simulations give only a slight overestimation of the wavelength shift for opals coated with 47 Å, 67 Å, and 100 Å of Al_2O_3 ALD. In contrast, the TMM results underestimate the Bragg wavelength shifts for the larger Al_2O_3 ALD thicknesses of 133 Å, 333 Å, 665 Å, 1330 Å, and 2660 Å.

The experimental measurements and the TMM simulations in Figure 5 both asymptotically approach a maximum wavelength shift. At this asymptotic limit, additional Al_2O_3 ALD does not affect the position of the Bragg wavelength. The TMM simulation results reach an asymptote after depositing 665 Å of Al_2O_3 ALD. In contrast, the experimental results reach an asymptote after depositing 1330 Å of Al_2O_3 ALD. The TMM simulations predict a maximum red shift

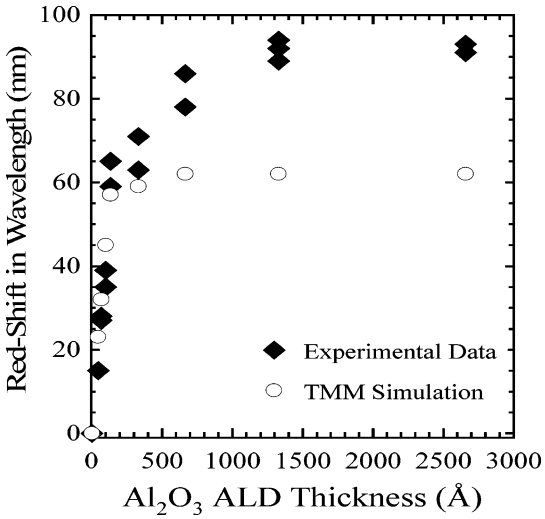

Figure 5. Shift in the Bragg wavelength versus Al_2O_3 ALD thickness for the experimental measurements and the TMM simulations. The initial Bragg wavelength is observed at $\lambda \sim 576$ nm. The experimental Bragg wavelengths shift much more than the Bragg wavelengths predicted by the TMM simulations.

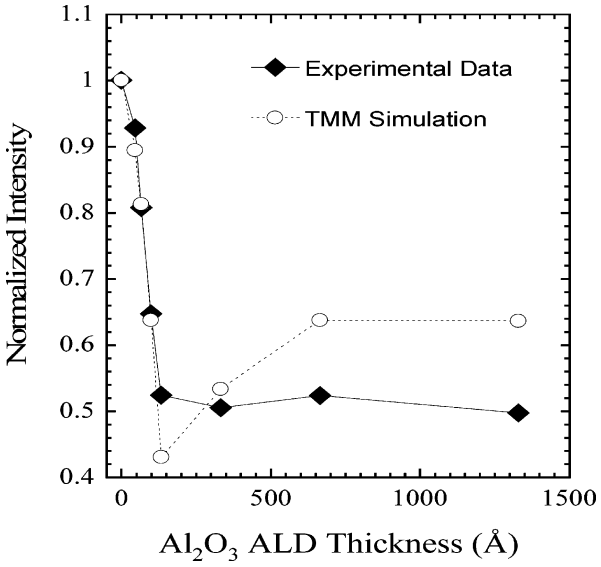

Figure 6. Experimental Bragg peak reflectances and the predictions from TMM simulations versus Al_2O_3 ALD thickness. The Bragg peak reflectances and predictions are both normalized for convenience in comparison.

of ~62 nm. The experimental results display a much larger maximum red shift of ~92 nm.

A drop in amplitude of the Bragg peak reflectance coincides with the red shift of the Bragg wavelength. The average intensities of the Bragg peaks for opal coated with varying amounts of Al_2O_3 ALD thickness are plotted in Figure 6. The intensities predicted by the TMM simulations are also shown for comparison. The intensities are normalized for convenience in comparing the experimental measurements and TMM predictions.

The intensity reduction is caused by the consumption of the volume fraction of air in the opal structure. Although the effective refractive index of the Al_2O_3 ALD-coated SiO_2 spheres increases, the volume fraction of air decreases as the air is displaced with Al_2O_3 ALD. The absolute refractive index difference between the SiO_2 spheres and the surrounding air/Al_2O_3 volume, $|n_{SiO_2} - n_{air/Al_2O_3}|$, decreases and then increases with decreasing volume fraction of air. These

(48) Vlasov, Y. A.; Deutsch, M.; Norris, D. J. *Appl. Phys. Lett.* **2000**, *76*, 1627.

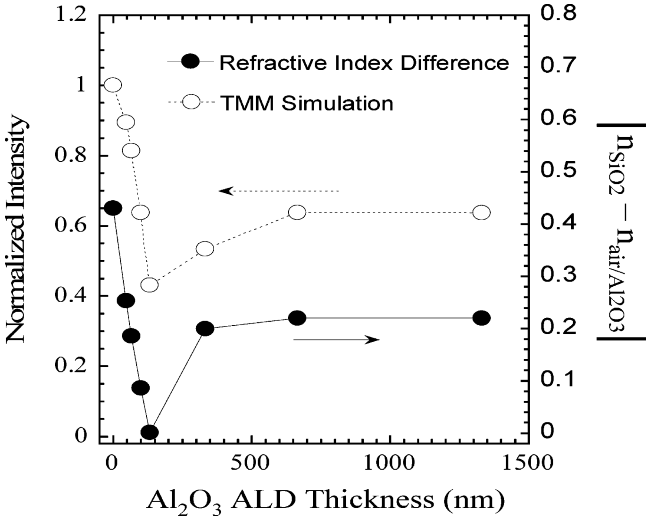

Figure 7. Comparison between the normalized Bragg peak reflectance from the TMM simulations and the absolute refractive index difference between the SiO_2 spheres of the opal structure and the surrounding air/Al_2O_3 volume versus Al_2O_3 ALD thickness.

changes occur because the refractive index difference is initially between SiO_2 ($n = 1.43$) and air ($n = 1.00$) and then between Al_2O_3 ($n = 1.65$) and SiO_2 ($n = 1.43$) after complete filling. At some point during the filling of the opal void volume with Al_2O_3 ALD, the refractive index of the air/Al_2O_3 volume is equal to $n = 1.43$ and the refractive index difference is zero. The changing absolute refractive index difference leads to a corresponding change in the Bragg peak reflectance.

The absolute refractive index difference between the SiO_2 spheres and the surrounding volume of air/Al_2O_3 is shown in Figure 7. The effective refractive index of the air/Al_2O_3 volume was defined using an equation similar to eq 5 with $F_{SiO_2} = 0$. The volume fractions of air and Al_2O_3 ALD were solved using Monte Carlo simulations with a perfect opal structure. The absolute refractive index difference and the TMM simulation intensities are in good agreement.

AFM images of an uncoated opal structure taken at different regions of the opal structure are shown in Figures 8 and 9. The image in Figure 8 shows a fairly well-ordered fcc (111) face of the opal crystal. Figure 9 shows a less ordered area of the opal crystal. Both images show silica spheres that vary slightly in size from one another. Figure 9 also shows site randomness that deviates more significantly from fcc geometry. The size and site randomness lead to a lower volume fraction of SiO_2 in the opal structure.

IV. Discussion

A. Al_2O_3 ALD on Opal as a Model System. Modifying photonic crystals, such as opals, demands a deposition technique that can conformally coat a structure that has a high aspect ratio. No other gas-phase techniques besides ALD can accomplish conformal coating on structures that do not have a line-of-sight to the source.[28] CVD can coat high aspect ratio structures only when the reactive sticking coefficient of one of the necessary precursors is extremely low.[49] Wet solution chemistry can be employed to deposit coatings on opal structures using techniques such as electroless plating.[18] Unfortunately, these techniques are difficult to control to obtain precise coating thicknesses.

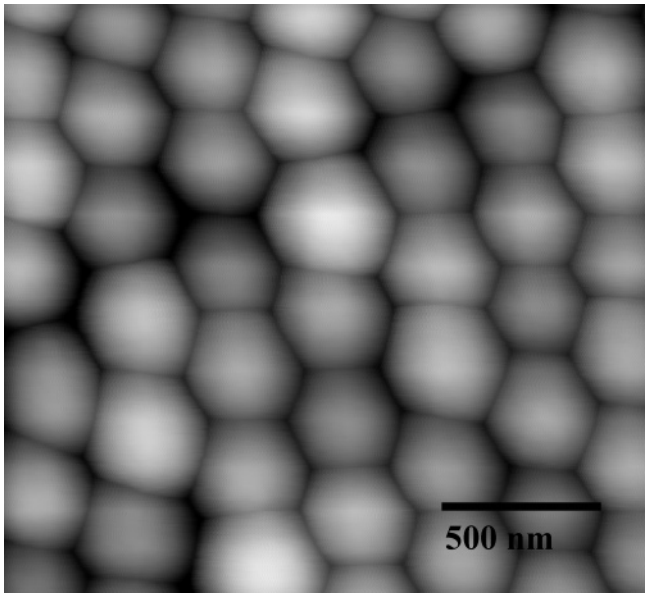

Figure 8. AFM image of a region of the opal structure that displays close-packed SiO_2 spheres.

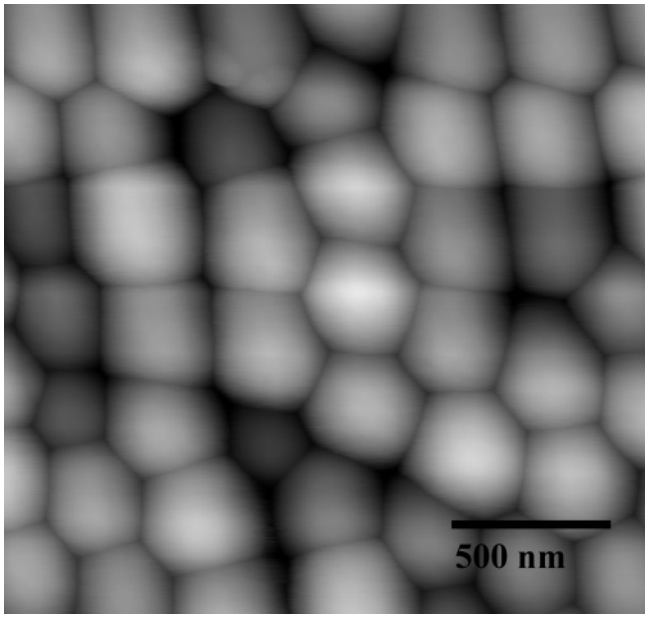

Figure 9. AFM image of another region of the opal structure that displays defects in the packing of the SiO_2 spheres.

Al_2O_3 ALD on opal was chosen in this study as a model system to understand the effects of ALD on the photonic properties of opal. Al_2O_3 ALD is a well-defined dielectric film with a higher refractive index than the SiO_2 spheres in opal. The properties and characteristics of Al_2O_3 ALD are very well-characterized by previous investigations.[30−33] The linear growth during Al_2O_3 ALD is illustrated in Figure 1. A similar linear growth is expected on the SiO_2 spheres of the opal structure if the reactant exposures are sufficient for the surface reactions to reach completion.[25]

The wavelength of the Bragg peak from the Al_2O_3 ALD-coated opal can be used to measure the effective refractive

(49) Islamraja, M. M.; Chang, C.; McVittie, J. P.; Cappelli, M. A.; Saraswat, K. C. *J. Vac. Sci. Technol. B* **1993**, *11*, 720.

index of the opal structure. Figure 4 shows that the wavelength of the Bragg peak shifts progressively to longer wavelengths versus Al_2O_3 ALD film thickness. This shift can be understood in terms of the simplified Bragg−Snell equation given by eq 4. The effective refractive index increases progressively as the higher refractive index of the Al_2O_3 ALD film adds to the lower refractive index of the SiO_2 spheres.

Figure 5 shows that the TMM simulations are in excellent agreement with the observed Bragg wavelengths versus Al_2O_3 ALD film thickness at low Al_2O_3 ALD thicknesses. These results illustrate the ability of Al_2O_3 ALD to tune the refractive index of the high aspect ratio opal structure. With a silica sphere diameter of 265 nm and an opal structure thickness of 2.5 μm, the estimated aspect ratio of the opal structure is ∼50. This estimate is based on the effective cylindrical pore diameter of ∼50 nm defined by the (111) fcc plane of the close-packed opal.

The conformal coating of Al_2O_3 ALD on the opal structure with an aspect ratio of ∼50 is not surprising given previous results. The sequential, self-limiting chemistry used in ALD has demonstrated very uniform, conformal coatings on extremely high aspect ratios. Previous ALD studies have observed conformal coating on aspect ratios as high as 5000:1.[28] ALDs to coat opal structures have been described earlier and demonstrated for ZnS ALD,[21] ZnO ALD,[22] WN ALD,[23] Ta_2N_5 ALD,[24] and TiO_2 ALD.[20] Each of these systems was believed to achieve a high volume fraction of ALD filling. However, none of these studies related the progressive change in the thickness of the ALD film to measurable optical properties.

An understanding of the connection between the optical properties and the thickness of the coating on each sphere in the opal is paramount for fine optical tuning of photonic crystals. The TMM simulation data shown in Figure 5 assumed that ALD films grow at identical rates on flat surfaces and on the spheres of the opal structure. The agreement between numerical simulations and experimental data for thin Al_2O_3 films suggests that this assumption is valid. This assumption can be extended to other ALD systems. This connection is especially important for the ALD of metals that cannot be easily monitored optically because of their high absorptivity.

B. Discrepancy between Measurements and Simulations. Figure 5 shows that the Bragg wavelengths from the experimental data and the TMM simulations are in good agreement at low Al_2O_3 ALD film thicknesses. However, the Bragg wavelengths from the experimental data and TMM simulations diverge for Al_2O_3 ALD film thicknesses greater than 133 Å. The TMM simulations predict that the red shift in the Bragg wavelength levels off at ∼638 nm for Al_2O_3 ALD thicknesses greater than 133 Å. In contrast, the experimental data observe that the red shift in the Bragg peak levels off at ∼668 nm for Al_2O_3 ALD thicknesses greater than 1330 Å.

The larger shifts in the wavelength of the Bragg peak than predicted by the TMM simulations imply a higher refractive index. These results indicate that more Al_2O_3 ALD was deposited in the opal structure than assumed by the simulations. The simulations assumed a fcc geometry for the opal structure and an initial free volume fraction of 0.26. The higher refractive index could be obtained by a larger initial free volume fraction than 0.26. This larger initial free volume would allow more Al_2O_3 ALD to fill the air space in the opal structure. The larger resulting Al_2O_3 ALD volume fraction would produce a higher effective refractive index for the opal structure that would yield a larger red shift for the Bragg peak.

Larger initial free volume fractions than 0.26 predicted for the fcc geometry have been observed previously.[10,47] These larger free volume fractions are expected if there are defects in the fcc structure. These defects could result from imperfect self-assembly that does not produce the close-packed fcc structure. All crystal structures that are not close-packed would lead to a larger free volume in the opal. The AFM image in Figure 9 reveals packing geometries that deviate significantly from the ideal close-packed fcc structure.

The larger Al_2O_3 ALD fill fractions could also result from smaller SiO_2 spheres in a fcc matrix of larger SiO_2 spheres. For example, only a 2% decrease in the SiO_2 sphere diameters with the same lattice constant would increase the free volume fraction from 0.26 to 0.30. Likewise, one sphere per unit cell in the opal that is 5% smaller would produce a free volume fraction of 0.29. The AFM images in Figures 8 and 9 show evidence for a distribution of SiO_2 sphere sizes. These smaller SiO_2 spheres observed in Figures 8 and 9 increase the open space volume in the fcc structure and would produce deviations in the ideal fcc structure.

The diameter of the spheres was determined to be $d \sim 255 \pm 13$ nm by SEM measurements. This diameter is lower than the diameter of $d \sim 265$ nm obtained by the TMM simulations. This diameter was obtained using a matrix of possible silica indices and various sphere diameters to obtain the Bragg peak at $\lambda = 576$ nm from the uncoated opal structure. A diameter of $d = 268 \pm 3$ nm was also obtained using the measured Bragg wavelength and assuming an effective SiO_2 refractive index of $n_{\text{eff}} = 1.32$ and an initial free volume fraction of 0.26. The difference between the SiO_2 sphere diameters obtained from the SEM and the Bragg peak measurements suggests that smaller SiO_2 spheres are enveloped in an approximate fcc crystal defined by larger SiO_2 spheres.

Equations 4 and 5 can be combined to yield

$$\lambda = 2a(n_{SiO_2}F_{SiO_2} + n_{Al_2O_3}F_{Al_2O_3} + n_{air}F_{air}) \qquad (6)$$

The filled SiO_2 volume fraction of the initial opal structure, F_{SiO_2}, and the spacing, a, between the (111) planes in the fcc crystal can be determined using the Bragg wavelengths corresponding to uncoated opal where $F_{Al_2O_3} = 0$ and the completely filled opal where $F_{air} = 0$. The Bragg wavelength is $\lambda = 576$ nm when $F_{Al_2O_3} = 0$ and $\lambda = 668$ nm when $F_{air} = 0$. These two equations can be solved for the two unknowns, F_{SiO_2} and a. This procedure yielded $F_{SiO_2} = 0.68$ and $a = 222$ nm.

The average spacing of $a = 222$ nm between the planes in the (111) direction yields a SiO_2 sphere diameter of $d = 273$ nm. This sphere diameter is higher than the sphere

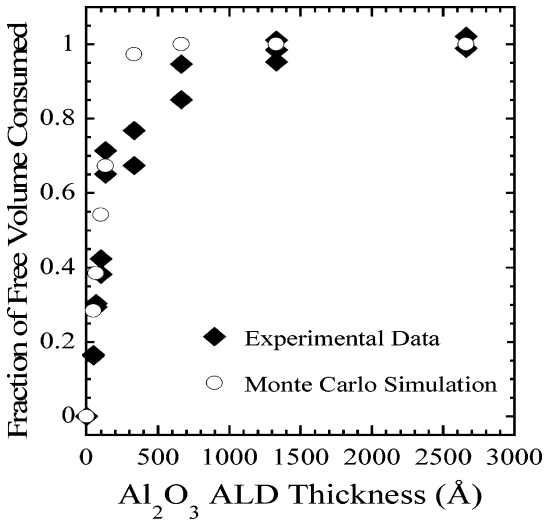

Figure 10. Fraction of free volume consumed versus Al_2O_3 ALD thickness. The experimental data is compared with Monte Carlo simulations assuming an ideal fcc structure.

diameters of $d = 255 \pm 13$ nm derived from the SEM measurements of individual spheres. This diameter is also slightly higher than the diameter of $d \sim 265$ nm obtained from the TMM estimate and $d = 268 \pm 3$ nm derived using the measured Bragg wavelength for the uncoated opal structure assuming an effective refractive index of $n_{eff} = 1.32$. The SEM measurements would be expected to be the lowest because they are measuring individual spheres. The diameters from the TMM estimates and Bragg wavelengths are averages over the assembled collection of spheres. These diameters would be larger than the diameters from the SEM measurements if smaller spheres can incorporate themselves into the lattice without significantly reducing the lattice parameter.

The filled volume fraction of $F_{SiO_2} = 0.68$ is considerably lower than $F_{SiO_2} = 0.74$ expected for a perfect fcc structure. The lower filled volume fraction indicates that the amount of free volume in the opal structure has increased from 0.26 to 0.32. This higher free volume can be filled by Al_2O_3 ALD. The resulting higher volume fraction of Al_2O_3 ALD will produce a larger effective refractive index and a larger red shift in the Bragg peak wavelength.

The wavelength of the Bragg peak determines the volume fraction of Al_2O_3, $F_{Al_2O_3}$, versus Al_2O_3 ALD thickness. The fraction of free volume consumed by Al_2O_3 ALD is equivalent to $F_{Al_2O_3}/0.32$. Figure 10 shows the fraction of free volume consumed versus Al_2O_3 ALD thickness. The fraction of free volume consumed by Al_2O_3 ALD asymptotically approaches 1.0 at an Al_2O_3 ALD thickness of 1330 Å. Figure 10 also shows the fraction of free volume consumed versus Al_2O_3 ALD thickness for the ideal fcc opal structure. These values were determined by Monte Carlo simulations assuming that the Al_2O_3 ALD thickness grew linearly with AB cycles. The fraction of free volume consumed asymptotically approaches 1.0 at a Al_2O_3 ALD thickness of 665 Å.

The difference between the asymptotic limits for the experimental data and those of the Monte Carlo simulations is partially explained by the larger initial free volume of 0.32 in the opal structure. The difference may also be attributed to the decreasing conductance for the gas reactants as the SiO_2 spheres are coated with Al_2O_3 ALD. The aspect ratio in the opal structure is increased as the Al_2O_3 ALD coats the spheres in the opal structure. The aspect ratio is defined as L/D, where L is the path length that the precursor must travel to reach the bottom of the opal structure and D is the diameter of the open gap between the Al_2O_3-coated SiO_2 spheres. The average height of the opal structure was 2.5 μm according to profilometry measurements. The diameter of the open gaps between the Al_2O_3 ALD-coated SiO_2 spheres approaches 0 with Al_2O_3 ALD thickness.

Previous investigations have studied the required exposures for ALD on high aspect ratio structures to reach completion and produce conformal deposition.[28,50] The required exposures depend on the aspect ratio according to $(L/D)^2$.[28,50] The Al_2O_3 ALD on the opal samples was performed using constant reactant exposures of 0.4 Torr·s. As the aspect ratio increases, at some point these reactant exposures will no longer be sufficient for conformal deposition on the opal structure. On the basis of the initial estimated aspect ratio of ~50, the exposure of 0.4 Torr·s was sufficient to deposit ~ 225 Å of Al_2O_3 ALD before reaching a partial conductance limit.[28]

Figure 6 shows that the reduction in the intensities of the experimental Bragg peaks and the TMM simulations are in excellent agreement at low Al_2O_3 ALD film thicknesses. The experimental Bragg peak intensities level out at Al_2O_3 ALD thicknesses > 133 Å. In contrast, the reflectance intensities predicted by the TMM simulations display a minimum at 133 Å and then increase at Al_2O_3 ALD thicknesses > 133 Å. The TMM simulations and the absolute refractive index difference shown in Figure 7 are in good agreement, and a minimum at 133 Å can be clearly observed. This minimum may not be observed in the experimental Bragg peak intensities because of sample variations and low reflectance signals for the large Al_2O_3 ALD thicknesses.

V. Conclusions

Aluminum oxide (Al_2O_3) ALD was examined on synthetic opal. This model system should be useful to understand the effects of ALD coatings on opal structures. The wavelength of the peak Bragg reflection from the photonic crystal was utilized to monitor the Al_2O_3 ALD. The wavelength of the peak Bragg reflection was observed to shift progressively to longer wavelengths versus Al_2O_3 ALD thickness. This red shift was explained by the increase in the effective refractive index of the opal structure as the higher refractive index Al_2O_3 coated the SiO_2 spheres in the opal structure. The wavelength asymptotically reached a limiting wavelength with the complete filling of the free volume of the opal structure with Al_2O_3 ALD. The decrease in intensity of the Bragg peak versus Al_2O_3 ALD thickness was explained by the decrease in the refractive index difference between the SiO_2 spheres and their surroundings. These results demonstrate that the location and intensity of the Bragg peak from photonic crystals can be tuned using ALD.

TMM simulations were used to predict the optical effects from the modified photonic crystal. The simulations assumed

(50) Gordon, R. G.; Hausmann, D.; Kim, E.; Shepard, J. *Chem. Vap. Deposition* **2003**, *9*, 73.

a fcc crystal structure with a free volume fraction of 0.26 and conformal Al_2O_3 ALD on the SiO_2 spheres in the opal structure. The comparison between the predicted and experimental Bragg wavelengths from the Al_2O_3-coated photonic crystals revealed excellent agreement for thin Al_2O_3 films. This agreement indicated that the Al_2O_3 ALD occurs conformally inside of the opal structure. Differences between the experimental and predicted Bragg wavelengths were larger for high filling fractions of the opal structure. A higher free volume in the opal structure than the free volume predicted by the fcc geometry can explain these discrepancies. Regions of the opal structure that contain smaller sphere diameters and regions of the structure that do not maintain the fcc geometry may account for this higher free volume. An initial free volume fraction of 0.32 in the original opal structure was determined based on the red shift in the Bragg peak wavelength.

Acknowledgment. This work was supported by the National Science Foundation through under Grant DMI-0304650 and by the NSF-ONR Navy Civilian Service Fellowship program. Additional resources were provided by the Air Force Office of Scientific Research.

CM060263D